Robust weakening of the Gulf Stream during the past four decades observed in the Florida Straits

Christopher G. Piecuch[1]* and Lisa M. Beal[2]

[1]Physical Oceanography Department, Woods Hole Oceanographic Institution, Woods Hole, MA, USA.
[2]Rosenstiel School of Marine and Atmospheric Science, University of Miami, Miami, FL, USA.

Key Points:

- We quantify changes in Gulf Stream volume transport through Florida Straits since 1982 by applying Bayesian methods to multiple datasets.
- Gulf Stream volume transport through Florida Straits declined by 1.2 ± 1.0 Sv during the past 40 years (95% credible interval).
- This represents the first unequivocal observational evidence for a recent multidecadal weakening of this climate-relevant ocean current.

*Christopher G. Piecuch, Physical Oceanography Department, Woods Hole Oceanographic Institution, 266 Woods Hole Road, Massachusetts, USA 02543

Corresponding author: Christopher G. Piecuch, cpiecuch@whoi.edu

Abstract

The Gulf Stream is a vital limb of the North Atlantic circulation that influences regional climate, sea level, and hurricane activity. Given the Gulf Stream's relevance to weather and climate, many studies have attempted to estimate trends in its volumetric transport from various datasets, but results have been inconclusive, and no consensus has emerged whether the current is weakening with climate change. Here we use Bayesian analysis to jointly assimilate multiple datasets from the Florida Straits to quantify uncertainty and change in Gulf Stream volume transport since 1982. We find with virtual certainty (probability $P > 99\%$) that Gulf Stream volume transport through the Florida Straits declined by 1.2 ± 1.0 Sv in the past 40 years (95% credible interval). This represents the first unequivocal evidence for a recent multidecadal decline in this climate-relevant component of ocean circulation.

Plain Language Summary

The Gulf Stream is a major ocean current located off the East Coast of the United States. It carries a tremendous amount of seawater and along with it heat, carbon, and other ocean constituents. Because of this, the Gulf Stream plays an important role in weather and climate, influencing seemingly unrelated phenomena from sea level along coastal Florida to temperature and precipitation over continental Europe. Given how important this ocean current is to science and society, scientists have tried to figure out whether the Gulf Stream has undergone significant changes under global warming, but so far, they have not reached a firm conclusion. Here we report our effort to synthesize available Gulf Stream observations from the Florida Straits near Miami, and to assess whether and how the Gulf Stream transport there has changed since 1982. We conclude with a high degree of confidence that Gulf Stream transport has indeed slowed by about 4% in the past 40 years. Our finding is the first conclusive, unambiguous observational evidence that this ocean current has undergone significant change in the recent past, and future studies should try to identify the cause of this change.

1 Introduction

The Gulf Stream is the western boundary current of the subtropical North Atlantic Ocean (Stommel, 1965). It flows north through the Florida Straits off Miami and along the continental slope of the South Atlantic Bight before detaching from the coast at Cape Hatteras and meandering freely into the open ocean (Heiderich and Todd, 2020). By virtue of its volume and heat transports, the Gulf Stream affects regional weather and climate as well as coastal conditions, including European surface air temperature and precipitation, sea level along the Southeastern United States, and North Atlantic hurricane activity (Donnelly et al., 2015; Little et al., 2019; Palter, 2015). Understanding past Gulf Stream changes is therefore important for interpreting observed changes and predicting future trends in extreme events including droughts, floods, heatwaves, and storms (Seneviratne et al., 2021).

Determining trends in Gulf Stream transport is also relevant for clarifying whether elements of the large-scale North Atlantic circulation have changed and determining how the ocean is feeding back on the global climate system (Jackson et al., 2022). The difference between the northward transport by the Gulf Stream and southward transport due to winds over the ocean interior defines the strength of the Atlantic meridional overturning circulation (McCarthy et al., 2019). The overturning circulation is the primary means by which the ocean moves heat across latitudes, cooling tropical regions and warming the poles (Lumpkin and Speer, 2007). Climate models predict that the Atlantic meridional overturning circulation has weakened by 1.2 ± 0.2 Sv since the 1980s due to human influence (Menary et al., 2020; Weijer et al., 2020), but reconstructions derived from the sparse hydrographic data available since the 1980s find no significant weakening (Caínzos et al., 2022; Fu et al., 2020; Worthington et al., 2021). It is unclear if the discrepancies reflect issues with the models (inability to resolve fronts, jets, eddies, etc.) or the data

(e.g., aliasing of the sparse hydrographic observations), or whether the signal of anthropogenically forced change is below the detection threshold set by natural variability (Jackson et al., 2022). While continuous direct observations of the overturning circulation are too short to corroborate the simulated weakening (McCarthy et al., 2019; Lobelle et al., 2020), estimates of Gulf Stream transport are available earlier in time.

There is a long history of Gulf Stream observations from remote sensing and *in situ* data along the current's path (Stommel, 1965). The longest, most continuous record of Gulf Stream transport is from Florida Straits at 27°N (Figure 1) (Baringer and Larsen, 2001; Meinen et al., 2010; Volkov et al., 2020). There, quasi-daily estimates from submarine telecommunications cables calibrated with regular shipboard hydrographic surveys extend from 1982 and satellite altimetry provides additional data constraints every ~ 10 days since 1992 (Figures 1, 2a). Despite the extraordinary density of data, there is, as yet, no consensus that Gulf Stream transport is weakening with climate change. Meinen et al. (2010) interrogated observations from free-falling floats and cable data at 27°N since 1982 along with earlier upstream float measurements from south of Northwest Providence Channel near 26°N. They argued that the data do not support a change in Gulf Stream transport over 1964–2009, but they did not quantify the longterm rate of change or provide error estimates. In contrast, Park and Sweet (2015) reported a transport trend equivalent to a weakening of 1.1±0.1 Sv from the cable data over 1982–2014. Yet, their calculation did not account for serial correlation of residual transports or the large, time-variable uncertainties on the cable data (Garcia and Meinen, 2014; Meinen et al., 2010; Volkov et al., 2020), and so their formal error bars were probably too small (Bos et al., 2014). Evidence from farther downstream along the Gulf Stream is also equivocal. Rossby et al. (2014) analyzed 20 years of direct velocity data at 70°W but found no evidence of a decrease in Gulf Stream transport over 1993–2012, whereas Dong et al. (2019) used satellite altimetry to infer a weakening east of 65°W during 1993–2016, but no change west of 70°W.

In summary, there have been many attempts to estimate Gulf Stream trends from various data sets, but a definitive answer has remained elusive. We propose that, to make a robust estimate of longterm change with meaningful error bars, the available data should be jointly assimilated in a way that accounts for the time series properties of the transport and the uncertainties characterizing the different data streams.

2 Methods

To quantify, with uncertainties, daily Gulf Stream transports at Florida Straits since 1982, we apply hierarchical Bayesian modeling (Cressie and Wikle, 2011) to transports from cable, hydrography, and altimetry at 27°N (Appendix). Hierarchical modeling is based on the notion of conditional probabilities (Berliner, 1996), and represents a mathematically coherent framework for jointly assimilating all the available data and modeling the sources of uncertainty that characterize the problem. Our Bayesian model consists of three submodels—the first is the process submodel representing the temporal evolution of the Gulf Stream transport, which we model as the sum of a linear trend, seasonal cycle, and autoregressive noise; the second is the data submodel, which prescribes the relationships between the true underlying transport process and noisy, gappy transports from the cable, hydrography, and altimetry; the third is the prior submodel that places initial constraints on the uncertain parameters in the process and data submodels. We bring these submodels together using Bayes' theorem, which allows us to propagate uncertainties across the various levels of the problem. We generate an ensemble of posterior solutions that provide a probabilistic, continuous description of Gulf Stream transport on daily to decadal timescales from 18 March 1982 to 06 December 2021 (Figure 2b, 2c). See the Appendices for more detailed descriptions of the data and the model.

3 Results

We find a mean transport of 31.8±0.27 Sv (95% posterior credible interval), which is more tightly constrained than the value of 32.1±0.4 Sv reported by Meinen et al. (2010), and lower than the value of 32.2 Sv from Baringer and Larsen (2001) based on a shorter cable record (1982–1998), since we assimilate longer, more recent data during a time when transport declined (see immediately below). While errors vary in time depending on data quality and availability, daily transport uncertainties (posterior standard deviations) are ~ 0.9 Sv on average, which is smaller than the standard errors on the daily cable data (Figure 2c, 2d).

We conclude that Gulf Stream transport in Florida Straits declined by 1.2 ± 1.0 Sv over the past 40 years (Figures 2e, 2f), which is equivalent to a change of 4.0±3.2% relative to the mean transport. The probability that Gulf Stream transport weakened more than expected from random chance is $P > 99\%$. This trend only recently emerged from the data. A set of sensitivity experiments where the Bayesian model was only given the data through 2005, 2009, 2013, and 2017 yielded respective transport-weakening probabilities of $P = 51\%$, $P = 79\%$, $P = 96\%$, and $P = 97\%$ (Figure 2e). This demonstrates that a significant decline in Gulf Stream transport has only become detectable during the past decade. The Gulf Stream transport decline from the Bayesian model is also robust across datasets. Omitting data from the cable, hydrography, or altimetry from the analysis, we determine weakenings of 0.8 ± 1.0, 1.1 ± 1.0, and 1.2 ± 0.9 Sv, respectively (Figure 2f). This shows that a very likely ($P > 94\%$) transport weakening is a common signal and not dependent on any one dataset.

4 Discussion

The 1.2±1.0-Sv transport weakening identified we find here is consistent with the 1.2 ± 0.2-Sv decline in the Atlantic meridional overturning circulation since 1980 due to human influence predicted by climate models (Menary et al., 2020; Weijer et al., 2020). However, it remains to determine whether wind-driven interior circulation also changed over the same time. Future studies could apply similar Bayesian methods to additional data to paint a fuller picture of past changes in North Atlantic circulation. For example, data from the RAPID array across the Atlantic since 2004 could be assimilated with temperature and salinity observations across the basin at 26°N and within Florida Straits to establish whether the Gulf Stream slowdown is associated with interhemispheric exchange by the meridional overturning or local recirculation by the subtropical gyre (Caínzos et al., 2022; Fu et al., 2020; McCarthy et al., 2019; Worthington et al., 2021). Folding temperature, salinity, carbon, and other tracers into a more expansive Bayesian model may also permit an inference on ocean heat and biogeochemical transports that are more directly relevant to climate (McCarthy et al., 2019). Our new Gulf Stream transport time series could also be used to investigate relationships between Gulf Stream transport and flooding along the Florida coastline, since it is made independently of coastal tide-gauge data (Sweet et al., 2015).

We find unequivocal evidence for a multidecadal decline of Gulf Stream transport in Florida Straits since the 1980s. Yet, this longterm weakening represents only a fraction of the variability and change in ocean transport. There is debate surrounding whether proxy reconstructions based on natural archives support a significant decline in North Atlantic circulation on longer centennial timescales since the Industrial Revolution (Caesar et al., 2022; Kilbourne et al., 2022), and shorter instrumental observational records of the meridional overturning circulation reveal strong decadal variability (Jackson et al., 2022; Moat et al., 2020; Smeed et al, 2019). These remaining ambiguities underscore the value of sustained longterm monitoring of ocean circulation and the importance of assimilating available observations within a hierarchical framework to rigorously quantify uncertainty and change.

Acknowledgments

Support came from NSF awards OCE-2123692/OCE-2123691 (Physical Oceanography), OCE-2002485 (P2C2), and NASA grant 80NSSC20K1241 (Sea Level Change Team). Woods Hole Oceanographic Institution is located on the unceded ancestral and contemporary land of the Wôpanâak (Wampanoag) peoples.

Open Research

All data used in this study were downloaded from the NOAA WBTS project website on 10 December 2021 (`https://www.aoml.noaa.gov/phod/wbts/`). The computer code used to run the Bayesian model and produce the results in this study is available at the CGP's GitHub website (`https://github.com/christopherpiecuch`).

Appendix A Data

The Florida Current represents the Gulf Stream at its headwaters in Florida Straits. Therefore, we use the phrases Florida Current and Gulf Stream at Florida Straits interchangeably, noting that the Gulf Stream's behavior is distinct at other latitudes upstream (Heiderich and Todd, 2020). We use observations of Florida Current volume transport from the National Oceanic and Atmospheric Administration Western Boundary Time Series (NOAA WBTS) project. All data were downloaded on 10 December 2021, including transport estimates determined from cable voltages, hydrographic cruises, and satellite altimetry.

A1 Cable

We use 13,105 quasi-daily Florida Current transport estimates from voltages measured across abandoned submarine telecommunications cables between Florida and The Bahamas. The principle is based on electromagnetic theory: oceanic transports of charged particles in the presence of earth's geomagnetic field result in variable across-cable voltages (Larsen, 1992). Data from 18 March 1982 to 22 October 1998 are from a cable between Jupiter Inlet and Settlement Point while the data from 9 June 2000 to the present are from a cable from West Palm Beach to Eight Mile Rock. No measurements were made from October 1998 to June 2000. The data are provided at daily resolution, but the effective sampling rate is three-daily, since the data are low-pass filtered to suppress geomagnetic effects and other noise. Cable estimates are calibrated against independent transport measurements from free-falling dropsonde floats and lowered acoustic doppler current profiler (LADCP) during cruises by the *R/V Walton Smith* across Florida Straits (Meinen et al., 2010; Garcia and Meinen, 2014). Volkov et al. (2020) compare the cable data to dropsonde observations and obtain standard errors on the former of 2.8 Sv for 1993–1998, 2.0 Sv for 2000–2005, and 1.3 Sv for 2006 onward. Larger errors for 1993–1998 and 2000–2005 result from the cables being in active telecommunications use and problems with the recording system, respectively (Meinen et al., 2010; Volkov et al., 2020).

A2 Hydrography

We use 388 direct observations of Florida Current transport from a variety of *in situ* hydrographic platforms. Of these, 247 are from free-falling dropsonde floats, 85 are from LADCP, 60 are from acoustically-tracked Pegasus floats, and 9 from Pegasus floats in dropsonde mode. Pegasus float measurements were made from 1982 to 1984 as part of the Subtropical Atlantic Climate Studies program (Molinari et al., 1985), while the observations from Pegasus floats in dropsonde mode were obtained during later campaigns between 1986 and 1988. Dropsonde and LADCP measurements began later in 1991 and 2001, respectively. All WBTS hydrographic observations are on hiatus since 2021 due

to permitting issues with The Bahamas. Meinen et al. (2010) and Garcia and Meinen (2014) provided a detailed discussion of these observations and their uncertainties.

A3 Altimetry

We use 979 Florida Current transport estimates based on satellite altimetry. Satellite altimeters observe the global sea-surface height field every ~ 10 days. By virtue of geostrophy, gradients in sea-surface height are coupled to surface geostrophic currents. Motivated by this relationship, Volkov et al. (2020) used sea-surface height differences from along-track altimetry data across Florida Straits to estimate Florida Current transport since January 1993. Those authors compared their altimetry-based transport estimates to data from cables, dropsondes, and LADCP, and derived a standard error on the ~ 10-daily altimetric estimates of ~ 2 Sv.

Appendix B Model

We develop a hierarchical Bayesian time series model to analyze Gulf Stream transport data from cable, hydrography, and altimetry. The algorithm design follows the paradigm established by Berliner (1996): a process level (submodel) encodes mathematical rules describing the temporal evolution of the process, a data level specifies relationships between the true underlying process and the imperfect data, and a prior level imposes constraints on the parameters in the process and data levels, which are uncertain. We relate the posterior probability of the process and the parameters given the data to the process, data, and prior levels using Bayes' theorem. See Cressie and Wikle (2011) and Gelman et al. (2006) for a detailed description of hierarchical Bayesian modeling.

We use autoregressive–moving-average (ARMA) models (Cryer and Chan, 2008) to describe the structure in the data. The model equations below are the result of data exploration and trial and error. We successively applied ARMA(p, q) models with p autoregressive terms and q moving-average terms to the observations, increasing the order (p, q) until the residuals were described by white noise (see below). We interpreted the lowest-order model producing white-noise residuals as the simplest model that could justifiably be applied to the data.

All model processes, data, and parameters are listed in Table A1.

B1 Process level

We represent the Gulf Stream volume transport process $\boldsymbol{T} = [T_1, \ldots, T_K]^{\mathsf{T}}$ in terms of a third-order autoregressive [AR(3)] process superimposed on a time mean, seasonal cycle, and linear trend

$$T_k - \boldsymbol{w}_k^{\mathsf{T}}\boldsymbol{\beta} = \sum_{i=1}^{3} \left[\rho_i \left(T_{k-i} - \boldsymbol{w}_{k-i}^{\mathsf{T}}\boldsymbol{\beta}\right)\right] + s_k, \tag{B1}$$

where $s_k \sim \mathcal{N}\left(0, \sigma^2\right)$ is a zero mean, independent and identically distributed random normal innovation with unknown variance σ^2; $k \in [1, K]$ is the index; $\boldsymbol{w}_k$ is the k^{th} column of the $[6 \times K]$ design matrix

$$\mathsf{w} = \begin{bmatrix} 1 & 1 & \cdots & 1 \\ t_1 & t_2 & \cdots & t_K \\ \cos\left(2\pi t_1/\tau_{\text{A}}\right) & \cos\left(2\pi t_2/\tau_{\text{A}}\right) & \cdots & \cos\left(2\pi t_K/\tau_{\text{A}}\right) \\ \sin\left(2\pi t_1/\tau_{\text{A}}\right) & \sin\left(2\pi t_2/\tau_{\text{A}}\right) & \cdots & \sin\left(2\pi t_K/\tau_{\text{A}}\right) \\ \cos\left(2\pi t_1/\tau_{\text{Sa}}\right) & \cos\left(2\pi t_2/\tau_{\text{Sa}}\right) & \cdots & \cos\left(2\pi t_K/\tau_{\text{Sa}}\right) \\ \sin\left(2\pi t_1/\tau_{\text{Sa}}\right) & \sin\left(2\pi t_2/\tau_{\text{Sa}}\right) & \cdots & \sin\left(2\pi t_K/\tau_{\text{Sa}}\right) \end{bmatrix}, \tag{B2}$$

where t_k is the k^{th} time and τ_{A} and τ_{Sa} are annual and semiannual periods, respectively; $\boldsymbol{\beta} = [\beta_1\ \beta_2\ \ldots\ \beta_6]^{\mathsf{T}}$ are unknown regression coefficients; and $\{\rho_1, \rho_2, \rho_3\}$ are the un-

known AR coefficients. Note that we scale and center the time such that $t_1 = -1$ and $t_K = 1$. Also note that the $\sim$ symbol is read "is distributed as" and $\mathcal{N}(a, b^2)$ is the normal distribution with mean a and variance b^2.

B2 Data level

B21 Hydrography

We assume the hydrographic data $\boldsymbol{x} = [x_1, \ldots, x_K]^\mathsf{T}$ correspond to the transport process $\boldsymbol{T}$ according to

$$x_k = T_k + d_k, \tag{B3}$$

where $d_k \sim \mathcal{N}\left(0, \delta_k^2\right)$ is random noise with zero mean and δ_k^2 is the data error variance. Similar to values in Volkov et al. (2020) and Garcia and Meinen (2014), we set $\delta_k^2 = (1.0 \text{ Sv})^2$ if the data value was taken by dropsonde, $\delta_k^2 = (1.5 \text{ Sv})^2$ if it was taken by LADCP, $\delta_k^2 = (1.0 \text{ Sv})^2$ if it was taken from Pegasus profiling float, and $\delta_k^2 = (1.0 \text{ Sv})^2$ if it was taken from Pegasus float in dropsonde mode.

B22 Cable

We represent differences between the cable data $\boldsymbol{y} = [y_1, \ldots, y_K]^\mathsf{T}$ and the transport process $\boldsymbol{T}$ using a second-order moving-average [MA(2)] model

$$y_k = T_k + \sum_{i=1}^{2} (\theta_i e_{k-i}) + e_k, \tag{B4}$$

where $e_k \sim \mathcal{N}\left(0, \epsilon_k^2\right)$ is random noise with zero mean, ϵ_k^2 is the data error variance, and $\{\theta_1, \theta_2\}$ are unknown MA coefficients. This model captures the fact that the errors on the cable estimates are not independent from one measurement to the next because three-day averaging is applied to the data. To obtain similar errors to Volkov et al. (2020) given the form of Eq. ($B4$), we set $\epsilon_k^2 = (0.9 \text{ Sv})^2$ for data before 1993, $\epsilon_k^2 = (2.0 \text{ Sv})^2$ for data over 1993–1998, $\epsilon_k^2 = (1.4 \text{ Sv})^2$ for data over 2000–2005, and $\epsilon_k^2 = (0.9 \text{ Sv})^2$ for data since 2006.

B23 Altimetry

We model the relationship between the altimetry data $\boldsymbol{z} = [z_1, \ldots, z_K]^\mathsf{T}$ and the process $\boldsymbol{U} = [U_1, \ldots, U_K]^\mathsf{T}$ as

$$z_k = U_k + f_k, \tag{B5}$$

where $f_k \sim \mathcal{N}\left(0, \omega_k^2\right)$ is random noise with zero mean and ω_k^2 is the data error variance. We set $\omega_k^2 = (2.0 \text{ Sv})^2$ following Volkov et al. (2020).

Altimetry observes sea-surface height, not transport *per se*. We assume that the process underlying the altimetry data $\boldsymbol{U}$ reflects a combination of effects related and unrelated to transport $\boldsymbol{T}$, which we model as

$$U_k - T_k = \phi\left(U_{k-1} - T_{k-1}\right) + g_k, \tag{B6}$$

where $g_k \sim \mathcal{N}\left(0, \tau^2\right)$ is a zero mean, independent and identically distributed random innovation of unknown variance τ^2 and ϕ an unknown AR coefficient.

B3 Prior/Parameter level

We place prior constraints on the set of model parameters to complete the model. Our approach is to use agnostic, uninformative prior distributions, which have little effect on the posterior solutions, but rather serve to initialize the sampling algorithm on roughly the right order of magnitude in solution space. All priors are listed in Table A1.

B4 Evaluating the posterior distribution

Given the process-, data-, and parameter-level equations and Bayes' rule, we assume the posterior distribution of the process and the parameters given the data can be expressed as follows

$$\begin{aligned} & p\left(\boldsymbol{T}, \boldsymbol{U}, \boldsymbol{e}, \boldsymbol{\beta}, \boldsymbol{\rho}, \boldsymbol{\theta}, \phi, \sigma^2, \tau^2 | \boldsymbol{x}, \boldsymbol{y}, \boldsymbol{z}\right) \propto p\left(\boldsymbol{\beta}\right) p\left(\sigma^2\right) p\left(\tau^2\right) p\left(\rho_1\right) p\left(\rho_2\right) p\left(\rho_3\right) \\ \times \quad & p\left(\theta_1\right) p\left(\theta_2\right) p\left(\phi\right) p\left(T_0\right) p\left(T_{-1}\right) p\left(T_{-2}\right) p\left(e_0\right) p\left(e_{-1}\right) p\left(U_0\right) \\ \times \quad & \prod_{k=1}^{K} \Big[p\left(x_k | T_k\right) p\left(y_k | T_k, \theta_1, \theta_2, e_{k-1}, e_{k-2}\right) p\left(z_k | U_k\right) p\left(U_k | T_k, U_{k-1}, T_{k-1}, \phi, \tau^2\right) \\ \times \quad & p\left(T_k | \sigma^2, \rho_1, \rho_2, \rho_3, \boldsymbol{\beta}, T_{k-1}, T_{k-2}, T_{k-3}\right) \Big], \end{aligned} \tag{B7}$$

where p is probability distribution function, $|$ indicates conditionality, $\propto$ indicates proportionality, $\boldsymbol{\rho} = \{\rho_1, \rho_2, \rho_3\}$, and $\boldsymbol{\theta} = \{\theta_1, \theta_2\}$.

We evaluate posterior solutions using Markov chain Monte Carlo (MCMC) methods. We sample from the full conditional distributions using a Gibbs sampler (Gelman et al., 2006). We run 20,000 iterations of the Gibbs sampler, where initial process values are set to zero, and initial parameter values are drawn from their respective prior distributions. To eliminate startup transients, we discard the first 10,000 "burn-in" draws. To reduce serial correlation of the remaining samples, we thin the chains by only keeping one out of every 50 samples. Our final results are based on five separate 200-member chains run to convergence and then concatenated together.

B5 Technical details on the model solution

B51 Convergence

We assess convergence by computing the $\hat{R}$ statistic from Gelman et al. (2006) based on between-sequence and within-sequence variance. Values $\hat{R} \sim 1$ indicate convergence. For all posterior scalar parameter solutions, $\hat{R}$ values are indeed ~ 1 (not shown), meaning that solutions are converged.

B52 Influence of priors

To quantify the influence of the prior distributions on the posterior solutions, we compute ratios between the widths of the 95% posterior and prior credible intervals. Values ~ 1 indicate that the posteriors are as wide as the priors, meaning that the priors strongly constrain the posteriors and not much additional has been learned from the data, whereas values $\ll 1$ identify that the posteriors are much narrower than the priors, implying that solutions are largely determined from the information content of the observations and relatively unaffected by prior belief coded into the model. For all scalar parameters, we obtain ratios $\ll 1$ (not shown), demonstrating that the priors have comparatively small influence on the posterior solutions.

B53 Residual analysis

The process- and data-level model equations include residual time series s_k, d_k, e_k, f_k, and g_k that we assume behave like white noise with respective variances σ^2, δ_k^2, ϵ_k^2, ω_k^2, and τ^2. To test if model solutions conform to these assumptions, we perform residual analyses (Cryer and Chan, 2008) and interrogate the posterior s_k, d_k, e_k, f_k, and g_k solutions. If the residuals are consistent with white noise, then they will show no temporal autocorrelation. However, if the residuals feature temporal structure, then it would indicate a violation of the model assumptions, and that the model does not capture the structure in the data.

Figure A1 shows examples of posterior residual time series and autocorrelation functions. The time series look more or less random and have magnitudes basically consistent with the expected variance. More quantitatively, we find that 95%, 90%, 98%, 97%, and 95% of posterior s_k, d_k, e_k, f_k, and g_k values are captured by the 95% credible intervals on simulations of zero-mean white noise with variances σ^2, δ_k^2, ϵ_k^2, ω_k^2, and τ^2. The autocorrelation functions demonstrate that the residuals exhibit no significant temporal structure. From this, we conclude that posterior solutions are consistent with underlying model assumptions, meaning that the design of our algorithm is appropriate given the data.

B5.4 Cross-validation

The posterior uncertainties on our daily transport estimates are roughly half the size of the standard errors on the quasi-daily cable measurements (Figure 2d). To test whether our uncertainty estimates are meaningful, we perform a four-fold cross-validation (Efron and Hastie, 2016). That is, we perform four additional data-assimilation experiments. In each experiment, we withhold a randomly selected quarter of the observations, so that every data point is withheld in one of the four experiments. Then, with the resulting solutions for the transport process, we use the data equations to predict observations for times corresponding to the withheld data and, by comparing the predicted observations to the withheld data values, we quantify the prediction errors of the model solutions and the coverage of the posterior credible intervals. The prediction errors should be comparable to standard errors on the respective data, and the credible intervals should envelop the correction fraction of true values ($\sim 90\%$ of the true values should be captured by the 90% posterior credible interval, etc.).

Based on these experiments, we determine mean prediction errors of 1.1, 1.6, and 2.3 Sv for the cable, hydrographic, and altimetric data, respectively. These values are roughly consistent with data error variances coded into the model (see above). We also obtain that 97%, 77%, and 84% of the the respective cable, hydrographic, and altimetric data values are within the 90% posterior credible intervals from the Bayesian model solution. These results demonstrate that our uncertainty estimates capture roughly the correct proportion of true values.

References

Baringer, M. O. & Larsen, J. C. (2001). Sixteen Years of Florida Current Transport at 27°N. *Geophys. Res. Lett.*, **28**, 3179–3182.

Berliner, M. L. (1996). Hierarchical Bayesian Time Series Models. *Maximum Entropy and Bayesian Methods*, 15–22.

Bos, M. S. et al. (2014). The effect of temporal correlated noise on the sea level rate and acceleration uncertainty. *Geophys. J. Int*, **196**, 1423–1430.

Caesar, L. et al. (2022). Reply to: Atlantic circulation change still uncertain. *Nat. Geosci.*, **15**, 168–170.

Caínzos, V. et al. (2022). Thirty Years of GOSHIP and WOCE Data: Atlantic Overturning of Mass, Heat, and Freshwater Transport. *Geophys. Res. Lett.*, **49**, e2021GL096527.

Cressie, N., & C. K. Wikle (2011). Statistics for Spatio-Temporal Data. Wiley, Hoboken, 588 pp.

Cryer, J. D., & K.-S. Chan (2008). Time Series Analysis: With Applications in R. Springer, New York, 491 pp.

Dong, S. et al. (2019). Slow down of the Gulf Stream during 1993–2016. *Sci. Rep.*, **9**, 6672.

Donnelly, J. P. et al. (2015). Climate forcing of unprecedented intense-hurricane activity in the last 2000 years. *Earth's Future*, **3**, 49–65.

Efron, B., & T. Hastie (2016). Computer Age Statistical Inference: Algorithms, Evidence, and Data Science. Cambridge, New York, 475 pp.

Fu, Y. et al. (2020). A stable Atlantic Meridional Overturning Circulation in a changing North Atlantic Ocean since the 1990s. *Sci. Adv.*, **6**, eabc7836.

Garcia, R. F. & Meinen, C. S. (2014). Accuracy of Florida Current Volume Transport Measurements at 27°N Using Multiple Observational Techniques. *J. Atmos. Ocean. Tech.*, **31**, 1169–1180.

Gelman, A., et al. (2006). Bayesian Data Analysis: Second Edition. Chapman & Hall/CRC, Boca Raton, 668 pp.

Heiderich, J. & Todd, R. (2020). Along-Stream Evolution of Gulf Stream Volume Transport. *J. Phys. Oceanogr.*, **50**, 2251–2270.

Jackson, L. C. et al. (2022). The evolution of the North Atlantic Meridional Overturning Circulation since 1980. *Nat. Rev. Earth Environ.*, **3**, 241–254.

Kilbourne, K. H. et al. (2022). Atlantic circulation change still uncertain. *Nat. Geosci.*, **15**, 165–167.

Larsen, J. C. (1992). Transport and heat flux of the Florida Current at 27°N from cross-stream voltages and profiling data: theory and observations. *Phil. Trans. R. Soc. Lond. A*, **338**, 169–236.

Laurindo, L. et al. (2017). An improved near-surface velocity climatology for the global ocean from drifter observations. *Deep-Sea Res.*, **124**, 73–92.

Little, C. M. et al. (2019). The Relationship Between U.S. East Coast Sea Level and the Atlantic Meridional Overturning Circulation: A Review. *J. Geophys. Res. Oceans*, **124**, 6435–6458.

Lobelle, D. et al. (2020). Detectability of an AMOC Decline in Current and Projected Climate Changes. *Geophys. Res. Lett.*, **47**, e2020GL089974.

Lumpkin, R. & Speer, K. (2007). Global Ocean Meridional Overturning. *J. Phys. Oceanogr.*, **37**, 2550–2562.

McCarthy, G. D. et al. (2020). Sustainable Observations of the AMOC: Methodology and Technology. *Rev. Geophys.*, **58**, e2019RG000654.

Meinen, C. S. et al. (2010). Florida Current transport variability: An analysis of annual and longer-period signals. *Deep-Sea Res.*, **57**, 835–846.

Menary, M. B. et al. (2020). Aerosol-Forced AMOC Changes in CMIP6 Historical Simulations. *Geophys. Res. Lett.*, **47**, e2020GL088166.

Moat, B. I. et al. (2020). Pending recovering in the strength of the meridional overturning circulation at 26°N. *Ocean Sci.*, **16**, 863–874.

Molinari, R. L. et al. (1985). Subtropical Atlantic Climate STudies: Introduction. *Science*, **227**(4684), 292–295.

Palter, J. B. (2015). The Role of the Gulf Stream in European Climate. *Annu. Rev. Mar. Sci.*, **7**, 113–137.

Park, J. & Sweet, W. (2015). Accelerated sea level rise and Florida Current transport. *Ocean Sci.*, **11**, 607–615.

Rossby, T. et al. (2014). On the long-term stability of Gulf Stream transport based on 20 years of direct measurements. *Geophys. Res. Lett.*, **41**, 114–120.

Seneviratne, S. I. et al. (2021). Weather and Climate Extreme Events in a Changing Climate. *In Climate Change 2021: The Physical Science Basis. Contribution of Working Group I to the Sixth Assessment Report of the Intergovernmental Panel on Climate Change [Masson-Delmotte, V. et al. (eds.)]*. Cambridge University Press, Cambridge, 1513–1766.

Smeed, D. A. et al. (2018). The North Atlantic Ocean Is in a State of Reduced Overturning. *Geophys. Res. Lett.*, **45**, 1527–1533.

Stommel, H. (1965). The Gulf Stream: A Physical and Dynamical Description. Cambridge University Press, Cambridge.

Sweet, W. et al. (2016). In Tide's Way: Southeast Florida's September 2015 Sunnyday Flood. *Bull. Am. Meteor. Soc.*, **97**(12), S25–S30.

Volkov, D. L. et al. (2020). Inferring Florida Current Volume Transport From Satellite Altimetry. *J. Geophys. Res. Oceans*, **125**, e2020JC016763.

Weijer, W. et al. (2020). CMIP6 Models Predict Significant 21st Century Decline of the Atlantic Meridional Overturning Circulation. *Geophys. Res. Lett.*, **47**, e2019GL086075.

Worthington, E. L. et al. (2021). A 30-year reconstruction of the Atlantic meridional overturning circulation shows no decline. *Ocean Sci.*, **17**, 285–299.

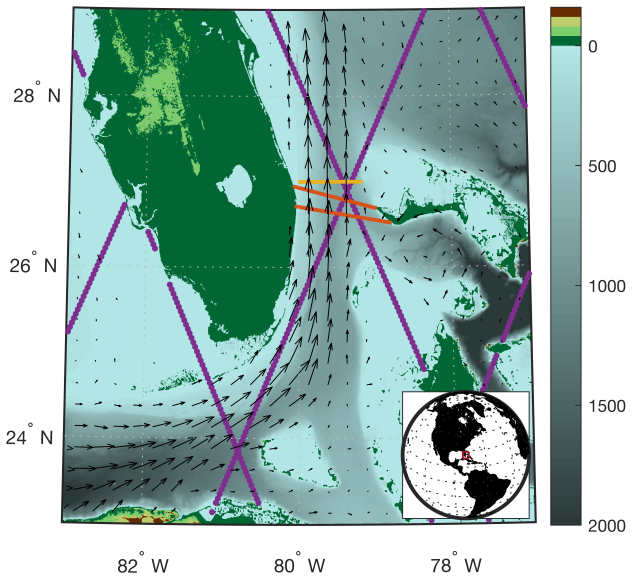

Figure 1. Study area. Color shading is topography/bathymetry (m) from the GEBCO 2021 grid. Orange lines mark nominal locations of submarine telecommunications cables between Jupiter Inlet (Florida) and Settlement Point (The Bahamas), and between West Palm Beach (Florida) and Eight Mile Rock (The Bahamas). Yellow line at 27°N marks nominal location of hydrographic sections. Purple dots mark altimeter ground tracks. Black arrows identify the relative magnitude and sense of the surface circulation from drifter observations (Laurindo et al., 2017). Inset shows the study area in global context.

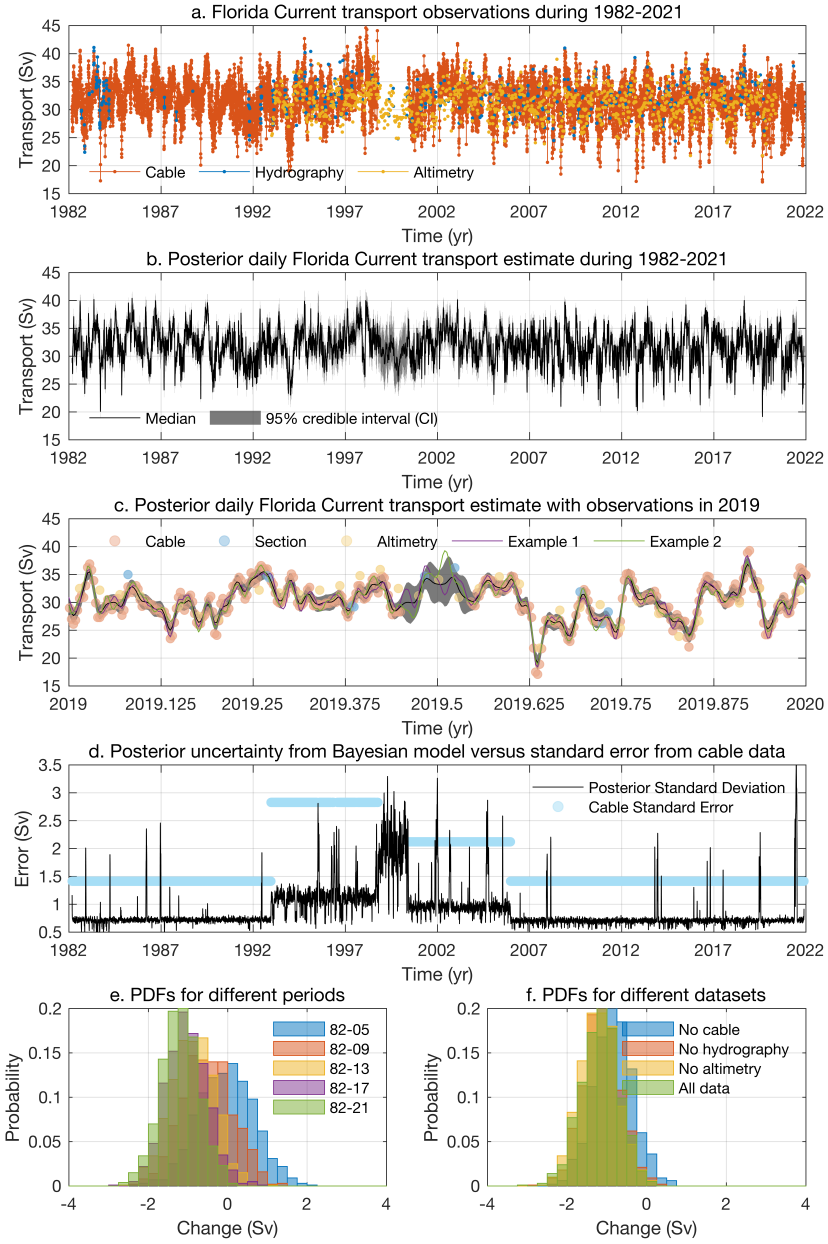

Figure 2. (a.) Observed Gulf Stream transport from undersea cable (orange), hydrography (blue), and satellite altimetry (yellow). (b.) Daily transport from the Bayesian model: posterior medians (black line) and 95% pointwise credible intervals (gray shading). (c.) Detail of observed (orange, blue, and yellow dots) and modeled (black line and gray shading) transport during 2019. Two randomly drawn posterior ensemble members are shown for comparison (purple and green lines). (d.) Posterior standard deviations on daily transports from the Bayesian model (black line) and standard errors on quasi-daily cable observations (cyan dots). (e.) Histograms of modeled transport change estimated over different time periods all starting in 1982. (f.) Histograms of modeled transport change over 1982–2021 estimated from experiments excluding each datasets from the analysis.

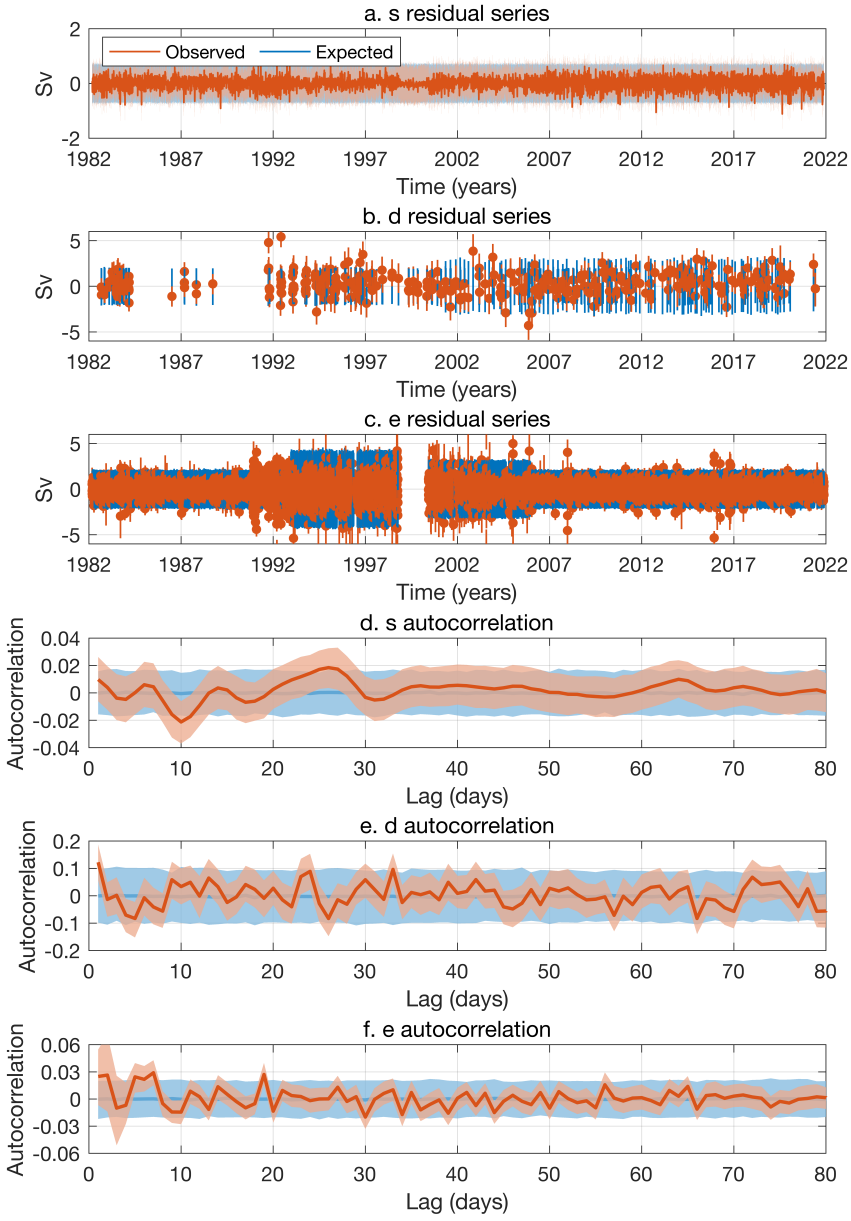

Figure A1. (a.) Orange shows medians (line) and 95% credible intervals (shading) for transport process residuals s_k determined empirically from the posterior model solution. Blue shading shows 95% credible intervals from simulations of random white noise with variance equal to posterior solutions of σ^2. (b.) As in (a.) but for hydrographic data residuals d_k and error variance δ_k^2. (c.) As in (a.) but for cable data residuals e_k and error variance ϵ_k^2. (d.) Orange shows medians (line) and 95% credible intervals (shading) on the autocorrelation function for the transport process residuals s_k determined empirically from the posterior model solution. Blue shows the autocorrelation function expected theoretically for white noise with the same degrees of freedom. (e.) As in (d.) but for hydrographic data residuals d_k. (f.) As in (d.) but for cable data residuals e_k.

Symbol	Description	Prior	Hyperparameters
T_k	Transport process	$p\left(T_i\right) \sim \mathcal{N}\left(\tilde{\mu}_0, \tilde{\zeta}_0^2\right)$ for $i \in \{-2,-1,0\}$	$\tilde{\mu}_0 = 30$ Sv, $\tilde{\zeta}_0^2 = 25$ Sv^2
U_k	Altimetric process	$p\left(U_0\right) \sim \mathcal{N}\left(\tilde{\mu}_0, \tilde{\zeta}_0^2\right)$	$\tilde{\mu}_0 = 30$ Sv, $\tilde{\zeta}_0^2 = 25$ Sv^2
x_k	Hydrographic data		
y_k	Cable data		
z_k	Altimetric data		
δ_k^2	Hydrographic data error variance		
ϵ_k^2	Cable data error variance		
ω_k^2	Altimetric data error variance		
s_k	Transport residual		
d_k	Hydrographic data error series		
e_k	Cable data error series	$p\left(e_i\right) \sim \mathcal{N}\left(0, \epsilon_0^2\right)$ for $i \in \{-1,0\}$	$\epsilon_0^2 = 0.81$ Sv^2
f_k	Altimetric data error series		
$\boldsymbol{\beta}$	Regression coefficients in transport process	$p\left(\boldsymbol{\beta}\right) \sim \mathcal{N}\left(\tilde{\boldsymbol{\mu}}_{\boldsymbol{\beta}}, \tilde{\mathsf{Z}}_{\boldsymbol{\beta}}\right)$	$\tilde{\boldsymbol{\mu}}_{\boldsymbol{\beta}} = [30,0,0,0,0,0]^{\mathsf{T}}$ Sv, $\tilde{\mathsf{Z}}_{\boldsymbol{\beta}} = 25\mathsf{I}_6$ Sv^2
ρ_i	Autocorrelation coefficient on transport process	$p\left(\rho_i\right) \sim \mathcal{N}\left(0, \tilde{\zeta}_\rho^2\right)$ for $i \in \{1,2,3\}$	$\tilde{\zeta}_\rho^2 = 0.25$ unitless
θ_i	Moving-average coefficient on cable data	$p\left(\theta_i\right) \sim \mathcal{N}\left(0, \tilde{\zeta}_\theta^2\right)$ for $i \in \{1,2\}$	$\tilde{\zeta}_\theta^2 = 0.25$ unitless
ϕ	Autocorrelation on transport-altimetry difference process	$p\left(\phi\right) \sim \mathcal{N}\left(0, \tilde{\zeta}_\phi^2\right)$	$\tilde{\zeta}_\phi^2 = 0.25$ unitless
σ^2	Variance of transport process	$p\left(\sigma^2\right) \sim \mathcal{IG}\left(\tilde{\xi}_\sigma, \tilde{\chi}_\sigma\right)$	$\tilde{\xi}_\sigma = 0.5$ unitless, $\tilde{\chi}_\sigma = 0.5$ Sv^2
τ^2	Variance of transport-altimetry difference process	$p\left(\tau^2\right) \sim \mathcal{IG}\left(\tilde{\xi}_\tau, \tilde{\chi}_\tau\right)$	$\tilde{\xi}_\tau = 0.5$ unitless, $\tilde{\chi}_\tau = 0.5$ Sv^2

Table A1. Descriptions of model processes, data, and parameters. Where applicable, priors and hyperparameters are also identified. $\mathcal{N}$ represents the normal distribution, $\mathcal{IG}(\xi, \chi)$ represents the inverse-Gamma distribution with shape ξ and scale χ, and I_6 is the 6×6 identity matrix.